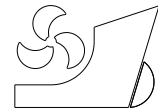


Omer Kemal KINACI
Metin Kemal GOKCE



ISSN 0007-215X
eISSN 1845-5859

A COMPUTATIONAL HYDRODYNAMIC ANALYSIS OF DUISBURG TEST CASE WITH FREE SURFACE AND PROPELLER

UDC 629.5.03:629.5.015.2:629.5.018.22

Original scientific paper

Summary

This paper discusses the effects of the free surface and the propeller on a benchmark Post-Panamax Ship, Duisburg Test Case (DTC). The experimental results are already available in the literature. The computational study carried out in this work is verified first with the experiments and then used to explain some of the physical aspects associated with viscous ship flows. There are two interesting outcomes of this work. The first one is, the existence of the propeller contributes to the pressure resistance of the ship by increasing the wave elevations along the hull and the fluid domain substantially. The second outcome is; by changing the pressure distribution along the hull and the propeller, the free surface increases the efficiency of the propulsion system. These specific outcomes are thoroughly discussed in the paper with CFD generated results and physical explanations.

Key words: *propulsion efficiency; ship resistance; effect of propeller; effect of free surface; Duisburg Test Case;*

1. Introduction

Flow around a bare hull with calm free water surface is one of the fundamental studies in naval architecture. The computational problem is around a century old which started with the foundation of potential theory at the start of 1900s. After maturing itself in time, potential theory also allowed the inclusion of free surface into the problem. With the developments in computer science, RANSE solvers were started to be used widespread which allowed solving for the viscous flows around ships. As the computer capabilities were extended, appendages were also included in the solutions.

Computational flow around a ship is one of the most challenging problems for the computational fluid dynamics (CFD) world. Ships are big structures that have complex geometries. Problems start from the beginning: it is really hard to have a good grid structure around the ship hull. The addition of an even more complex geometry, which is the propeller, complicates the grid problem.

The solution process involves two phases: air and water. The existence of free surface is another problematic issue for the ship hydrodynamicists. The rotating propeller at the aft of the ship needs special care due to its dynamics. Cavitation is a phenomenon that must be taken into

account because it has effect on the propulsion efficiency of the ship. Due to all these problems, naval architects who are working on ship hydrodynamics are usually more concentrated in solving this complicated flow and improving the obtained results. The underlying physics is generally not investigated by the CFD users. However CFD application to real ship flows has matured itself in time. Some results can be found in the open literature and a wide range of CFD results with various methods are given in Larsson et al. [1] for benchmark ships, KRISO Tanker (KVLCC2), KRISO Containership (KCS) and US Navy Combatant (DTMB 5415). Experiments usually reveal the physics behind a surface-piercing and propelling ship. However when used correctly, CFD may provide an invaluable tool to understand the flow around ships. CFD has matured itself in the last couple of decades and it is believed that it is possible to investigate the hydrodynamics of a ship computationally.

This paper discusses the effects of free surface and propeller on the hydrodynamics of a benchmark ship computationally. The ship used in this study is the Duisburg Test Case (DTC) which is a Post-Panamax Container Ship. The experimental results were published in [2]. The CFD generated results are first verified and then used to evaluate the computational outcomes. The free surface and the propeller are included in the solutions but the possible effects of cavitation are neglected.

2. Details of CFD approach

2.1 CFD setup

All the computational analyses are steady state solutions in this paper and $k - \varepsilon$ turbulence model is used with a commercial CFD code, ANSYS Fluent. This turbulence model is applicable when there are not high adverse pressure gradients along the hull. It is not as good as $k - \omega$ turbulence model when capturing the separation points. However $k - \omega$ needs lower $y +$ values along the hull to demonstrate its abilities and demands more computational power. Considering that the length-to-beam ratio of the benchmark vessel is $L/B = 7$, the vessel is considered to be slender and boundary layer separation along the hull is not playing an important role in the flow. Details of $k - \varepsilon$ turbulence model are given in [3].

To track the free surface boundary, volume of fluid (VOF) method is used. Rhee et al. [4] discusses that VOF “performs well for a wide range of free-surface wave types” and is a better option when compared to other available methods. The theory of VOF is given in [5].

2.2 CFD verification and validation

Three grid types were used to do CFD verification as established in [6, 7]. The total resistance coefficient of the bare hull was taken at $Fr = 0.218$ as the integral variable of the verification. The element numbers in these grids are deviated according to the Richardson extrapolation technique following the methodology of [6]. The properties and the generated results for different grid types are provided in table 1. The total numerical uncertainty U_N is given as

$$U_N = \sqrt{U_I^2 + U_G^2} \quad (1)$$

Here, U_I and U_G refer to iterative and grid uncertainties. All three cases have achieved oscillatory iterative convergence; therefore, the iterative uncertainty U_I was calculated as

$$U_I = \frac{1}{2} |S_U - S_L| \quad (2)$$

In table 1, S_U and S_L refer to the upper and lower values of total resistance in the simulations respectively. S_G is calculated as

$$S_G = \frac{1}{2} |S_U + S_L| \quad (3)$$

Table 1. Grid properties and their uncertainties.

	GRID 3	GRID 2	GRID 1
Element no.	447,000	1,286,000	3,468,000
$S_U \cdot 10^3$	5.236	4.449	4.409
$S_L \cdot 10^3$	5.057	4.394	4.407
$S_G \cdot 10^3$	5.1465	4.4215	4.408
$U_I \cdot 10^3$	0.0895	0.0275	0.001

By taking into account these three grids, the grid uncertainty and grid correction factor as proposed in [6, 7] are calculated as $U_G = 0.0267 \cdot 10^{-3}$ and $C_G = 52.7$ respectively. The grid uncertainty is about 25 times greater than the iterative uncertainty of grid 1. Therefore, it can be said that $U_N \cong U_G$ and,

$$U_N \cong 0.0267 \cdot 10^{-3}$$

The grid correction factor C_G is *sufficiently less than or greater than 1*, therefore results of grid 1 is used for the rest of this study without making any corrections.

The experimental result provided in [2] at $Fr = 0.218$ is $C_{T_{exp}} = 3.67 \cdot 10^{-3}$ while in grid 1 we get $C_{T_{grid1}} = 4.408 \cdot 10^{-3}$, which tells that the error is $E = 0.738 \cdot 10^{-3}$. For validation purposes, the error E has to be smaller than the validation uncertainty U_V . Validation uncertainty is given as

$$U_V = \sqrt{U_N^2 + U_E^2} \quad (4)$$

U_E refers to the experimental uncertainty. In the reference paper where the experimental results are published [2], the experimental uncertainty is not provided. However, it must be noted that the numerical uncertainty is very small as compared to the error. To satisfy $|E| < |U_V|$, the experimental uncertainty should be of the order of the error. Here there are two options. Either the experimental values provided in the reference paper have a large experimental uncertainty, or there is a bias of resistance forces calculated by the RANSE solver. To understand which one holds true, grid 1 is tested with other Froude numbers as well. This is covered in the next section and figure 4 plots the experimental and numerical total resistance curves. It is found out that the numerical method deployed in this study has a bias of results with the experimental study. The reason of this difference in the results might be accounted to the fixed body condition applied numerically while in the experiments the hull was free to sink and trim. In 1994, an 8% increase in total resistance coefficient for the fixed body condition for Series 60 was reported in [8]. Toda et al. [9] used fixed body condition for resistance computations around the Series 60 and calibrated their values by reducing 8% of the total resistance. It is possible that the same phenomenon also applies here which would let the resistance values get closer to the experimental results, if such calibration was performed.

2.3 Hydrostatics of the benchmark ship used in calculations

The Duisburg Test Case (DTC), which is a Post-Panamax Container Ship, is used in all the analyses involved in this paper. The experiments are carried out in the model basin SVA Potsdam and the results are given in [2]. The hydrostatic properties of the model ship are given in table 2. The domain size in all the analyses are chosen to meet the minimum requirements recommended by the ITTC [10] and are also listed in the same table.

Table 2. Hydrostatic properties of DTC [2] and the selected computational domain size.

Length between perpendiculars	L_{pp}	(m)	5.976
Waterline breadth	B_{wl}	(m)	0.859
Draft	T	(m)	0.244
Displacement	V	(m ³)	0.827
Block coefficient	C_B	-	0.661
Wetted area	S_W	(m ²)	6.243
Design speed	v_d	(knots)	3.244
Computational Domain Length	6*L _{wl}		
Computational Domain Width	1.5*L _{wl}		
Computational Domain Depth	L _{wl}		

3. Comparison of experimental results versus CFD approach

3.1 Bare hull resistance tests

The analyses involving the ship hull in this paper are made two ways. One is the double body flow solution which only covers the underwater hull (and the propeller if it exists). In this case only water exists (single phase) and the free surface is absent. The other covers the region outside the water as well and has the free surface interface between the air and the water (multi-phase). Validations in this study are made for both analysis types. Comparisons with the double body flow solutions are made with the ITTC correlation formula given for the frictional resistance coefficients [11]. Multi-phase solutions (which include the free surface) are validated by the experimentally obtained total resistance values given in [2].

The double body flow solutions are compared with the ITTC Correlation Line dictated by the ITTC57. Only the underwater hull is modeled due to the calm water assumption of the double body flow. The grid around the hull is given in figure 1. The comparison of frictional resistance coefficient, C_F , is given in figure 2.

Due to the complexity of the hull hybrid meshing is preferred. In a surrounding block which covers the hull, tetrahedral elements are used for practicality. This may be seen in figure 3. The rest of the domain has hexahedral elements which improve acquiring a better free surface deformation [12]. The computational total resistance and total resistance coefficient comparisons in contrast with the experimental values are given in figure 4. In terms of the total resistance coefficients, greater agreement is achieved with the experimental results at higher Fr numbers. Maki et al. [13] explain this with the nonlinear theory (RANS) being unable to correctly solve for the highly steeped waves which happen in lower Fr numbers. Same phenomenon is also observed in [14] where the discrepancy in low Fr numbers is more significant.

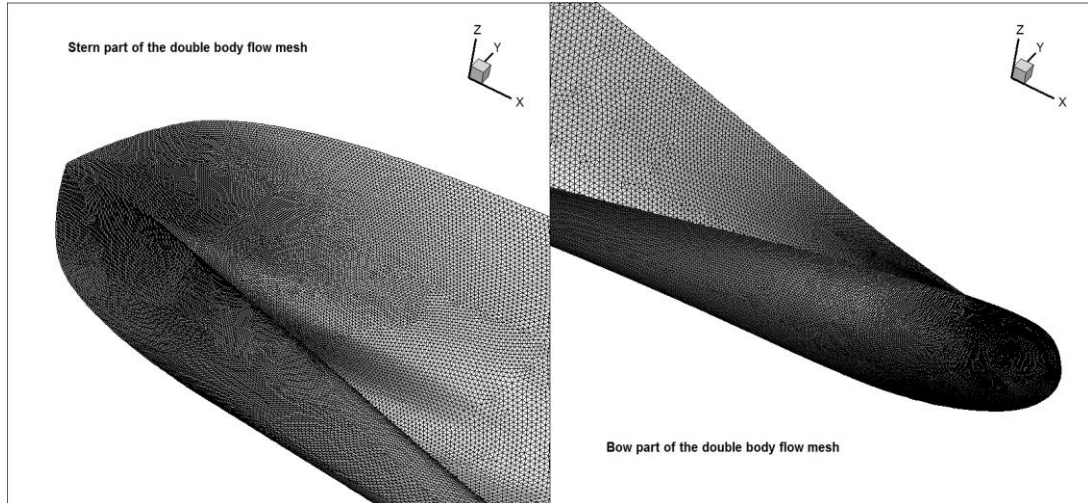


Fig. 1 – The grid around the stern part of the hull (left) and the bow part of the hull (b).

The total resistance coefficient values obtained by double body flow simulations (ignoring free surface) are also plotted in figure 4. It may be quickly noticed that the double body results are in very good accordance with the experimental results. However this is a fluke, because double body flow results do not include the wave resistance. Returning back at figure 2, it will be seen that CFD overpredicts the frictional resistance which compensates for the absence of wave resistance in double body flow simulations.

The obtained results for both the double body flow (which is a single phase analysis due to involving water only) and the multi-phase flow are found to be satisfactory. In both cases, CFD predicts higher resistances but the general shapes of the resistance curves are similar.

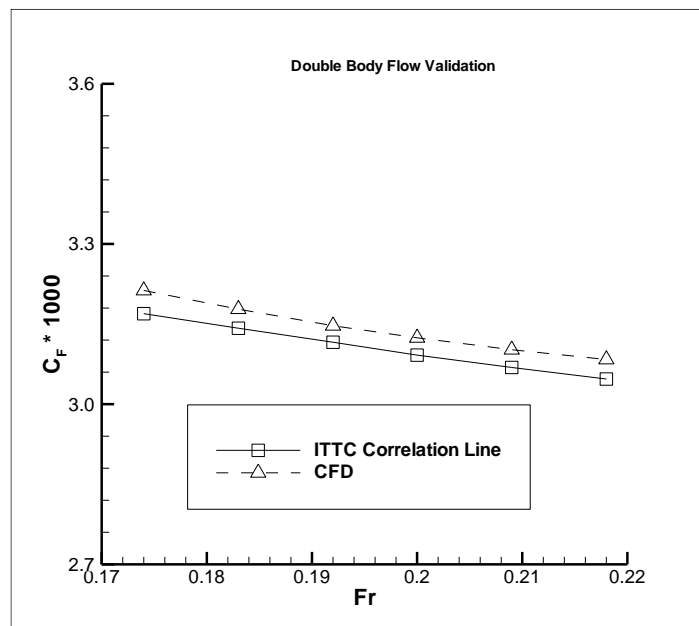


Fig. 2 – Comparison of frictional resistance coefficients obtained by ITTC57 and CFD.

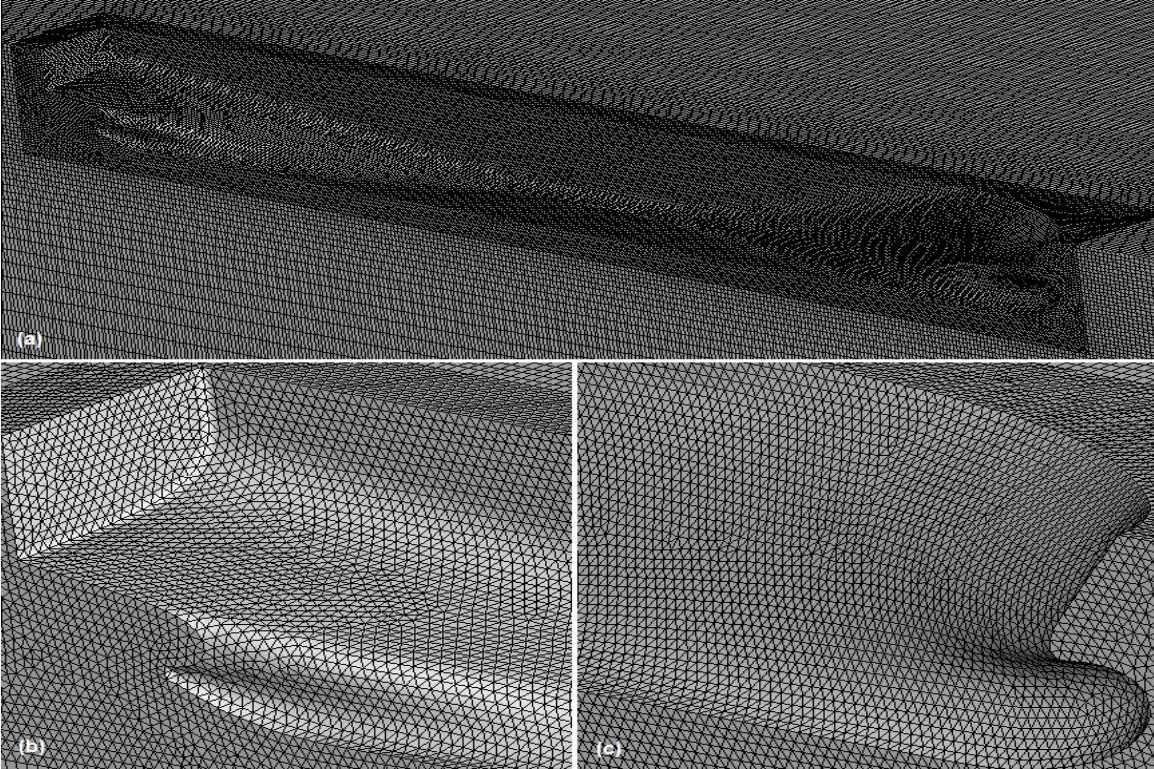


Fig. 3 – The grid around the hull (a) and stern (b) and the bow (c) for multi-phase flows.

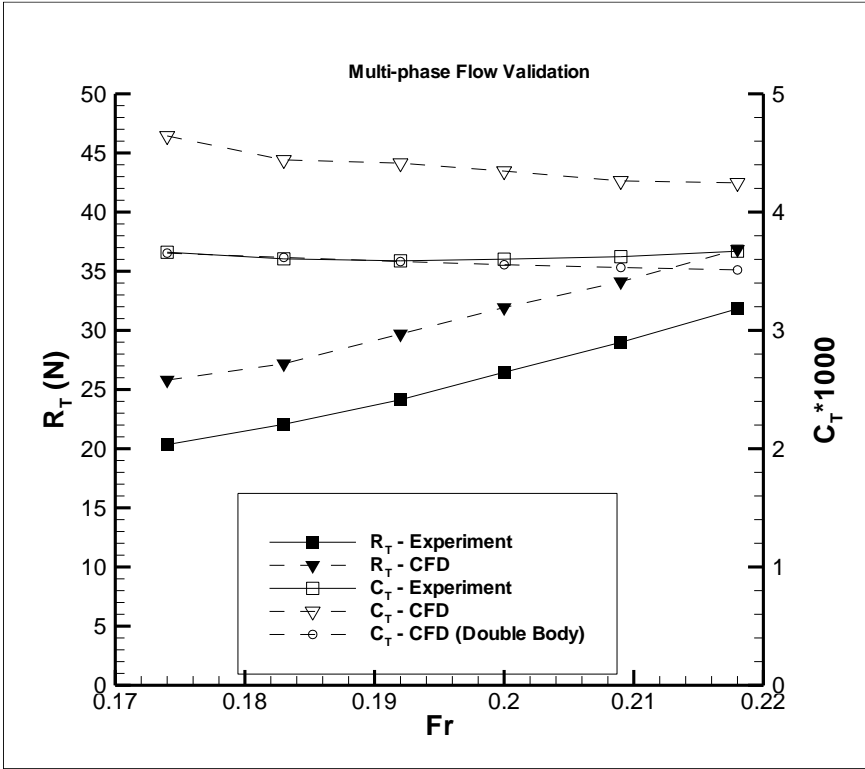


Fig. 4 – Comparison of total resistance and total resistance coefficient obtained by CFD and experiments [2].

3.2 Open-water propeller tests

The validation for resistance tests are explained above using two different analysis methods. However, due to the existence of propeller in some analyses in the following sections, a validation for solving the flow around the propeller is also needed. Open-water experimental results are used to verify the validity of the method used to treat the flow around the propellers. Figure 5 shows the mesh structure on the propeller surface used in the simulations. The diameter of the model propeller is $0.15m$ to be in accordance with the reference article [2]. The propeller is right-oriented and its parameters in detail are given in the same paper.

Propellers have complex geometries and therefore, once again, tetrahedral elements are preferred for easier meshing. The comparison of the computational results with the experiments is given in figure 6. It is found out that a very good agreement with the experimental results is obtained by CFD. For a detailed analysis on DTC propeller, see [15].

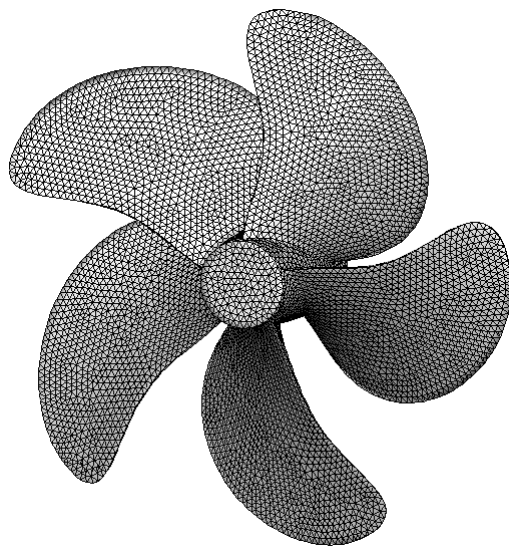


Fig. 5 – The grid on the propeller surface.

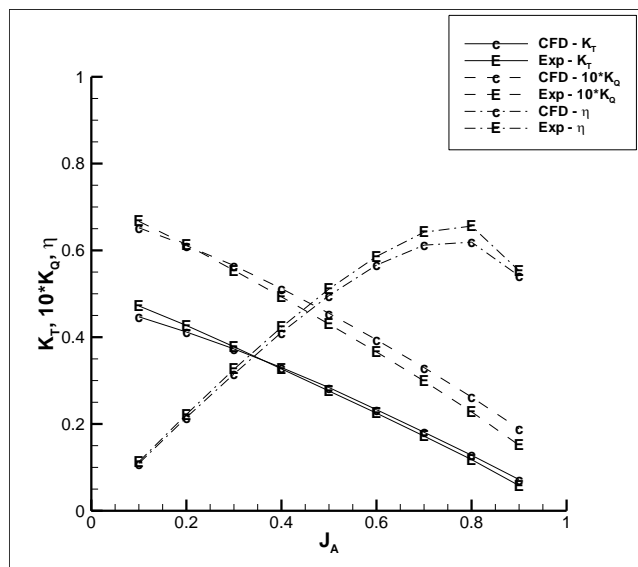


Fig. 6 – Comparison of CFD and experiments in terms of propeller characteristics.

4. Effect of the propeller in ship flow

4.1 Wave cut with and without the propeller

The wave characteristics of the ship were calculated with and without the propeller. In the case of the existence of the propeller, the hull-propeller system was subjected to different propeller rotations calculated by tentative advance coefficients. The advance coefficients of the propeller and the resistance components of the hull-propeller system along with the generated thrust by the propeller are given in table 3.

Due to the rotating nature of the propeller, it creates an asymmetry in the flow around the ship. This may be examined by observing the free surface elevation over the hull. In figure 7, it may be seen that the wave pattern along the hull is not the same at both sides of the ship in the case with the propeller. The wave elevations are equal at both sides of the ship when the propeller is absent because there is nothing in the flow that creates asymmetry. It must be noted here that the advance coefficient of the propeller is $J = 0.7$, and the wave elevations are expected to be slightly different in other advance coefficients.

It may be observed from figure 7 that the existence of the propeller increases the wave height along the hull except the stern region. The propeller sucks up the flow to create thrust, decreasing the amount of water at the aft of the ship. Due to the accelerated movement of water at this region, the pressure decreases. When the amount of water is reduced and the pressure is decreased, air replaces the places evacuated by the water; lowering the wave height at this part of the hull. The sucked up water at the aft part of the ship is compensated by the additional water at the bow region. This is one of the reasons of higher wave elevation at the front parts of the ship. The other reason is the additional resistance effect of the existence of the propeller.

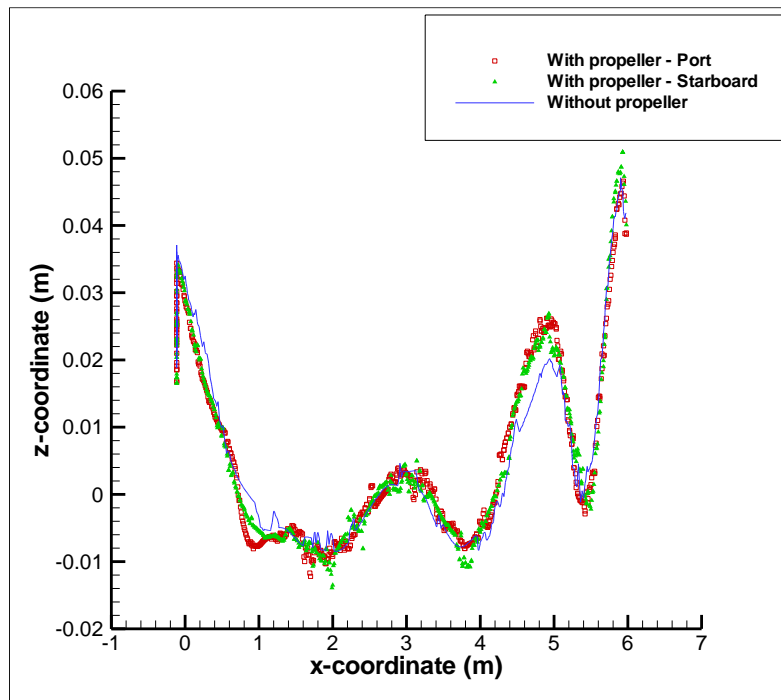


Fig. 7 – Wave elevations on the ship hull with and without the propeller at $Fr = 0.218$. For the case with the propeller, $J_S = 0.7$.

This additional resistance can numerically be observed from table 3. The table is created by changing the advance coefficient of the propeller and calculating the resistance and thrust values they generate. Lower advance coefficients have higher rotation and when the advance coefficient is infinite, this means that there is practically no existing propeller. In the table it may be seen that while the frictional resistance sails around a fixed value, the pressure resistance consistently drops. This supports the idea that when the propeller speeds up the flow and decreases the pressure at the stern of the ship, the pressure resistance increases. Table 3 also explains why the wave elevations are higher for the case with the propeller because wave resistance is a part of the pressure resistance.

The ejected water from the propeller causes higher waves at the wake of the ship. Figure 8 represents the wave elevations at the upstream and the downstream with and without the existence of the propeller at $y = 0$. Although there is not a major change at the upstream of the ship hull (which is not expected), there is a significant increase in wave height at the downstream of the hull. It is expected that wave elevations are decreased when the propeller works at higher advance ratios or the submergence depth of the propeller is increased. The free surface contours with and without the propeller in the whole fluid domain are given in figure 9. The propeller changes the generated waves in the fluid domain considerably.

Table 3. Numerical values of resistance and thrust at different advance coefficients for $Fr = 0.218$.

J_s	R_p (N)	R_f (N)	R_t (N)	T (N)	C_p	C_f	C_t
0.3	27.433	26.146	53.58	263.98	3.16E-03	3.01E-03	6.18E-03
0.4	22.079	26.081	48.16	136.01	2.55E-03	3.01E-03	5.55E-03
0.5	19.11	26.009	45.12	78.8	2.20E-03	3.00E-03	5.20E-03
0.6	17.435	25.968	43.4	48.69	2.01E-03	2.99E-03	5.01E-03
0.7	16.233	25.934	42.17	31.25	1.87E-03	2.99E-03	4.86E-03
0.8	15.151	25.904	41.06	20.49	1.75E-03	2.99E-03	4.73E-03
0.9	14.761	25.9	40.66	13.43	1.70E-03	2.99E-03	4.69E-03
1	14.37	25.908	40.28	8.55	1.66E-03	2.99E-03	4.64E-03
1.1	14.022	25.903	39.92	5.08	1.62E-03	2.99E-03	4.60E-03
1.2	13.558	25.892	39.45	2.46	1.56E-03	2.99E-03	4.55E-03
infinity	10.584	26.058	36.84	0	1.22E-03	3.00E-03	4.25E-03

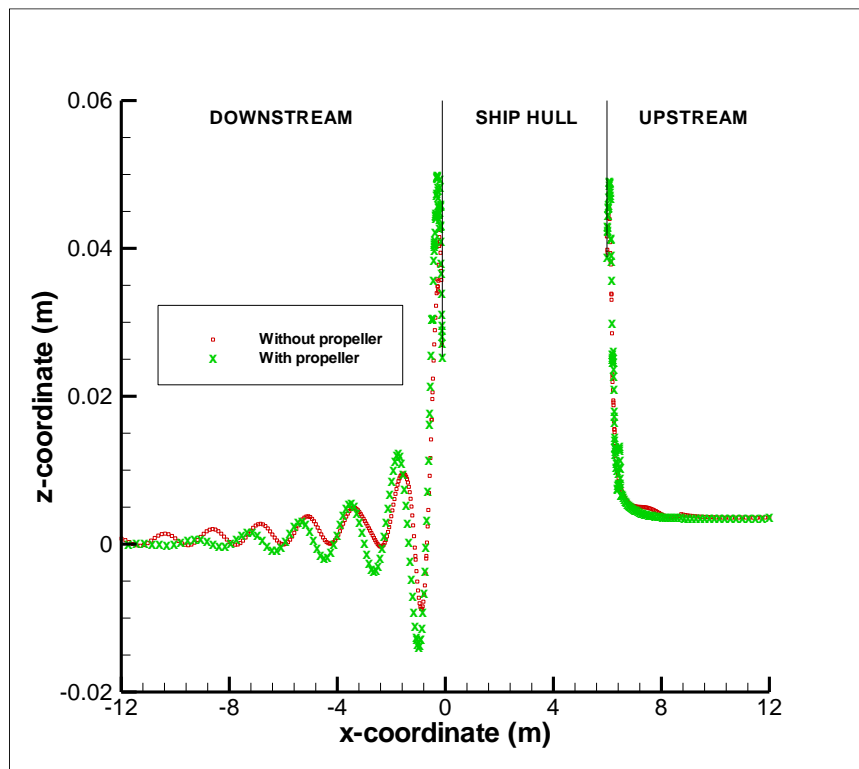


Fig. 8 – Wave cut at $y = 0$ of the fluid domain for $Fr = 0.218$.

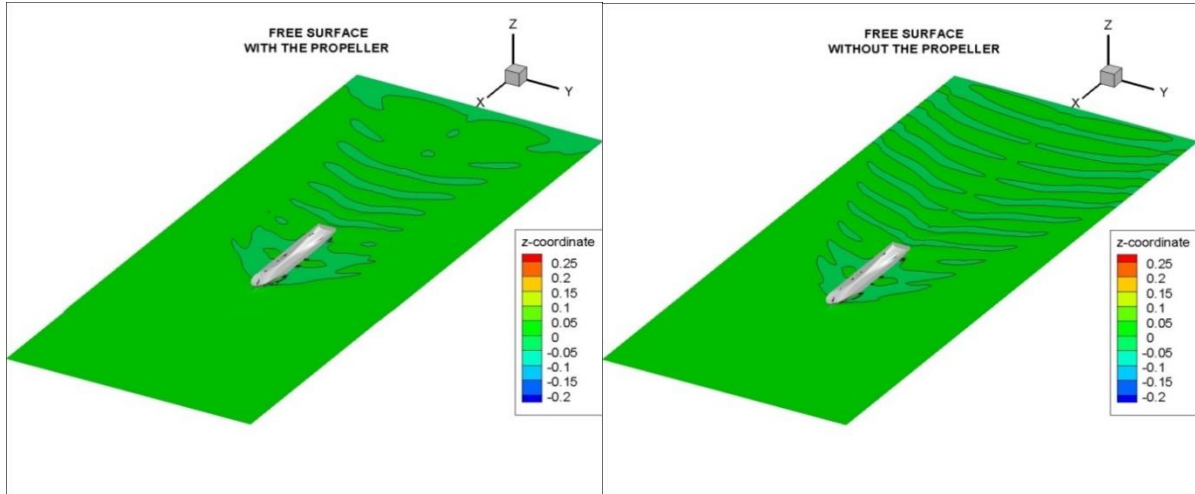


Fig. 9 – Free surface contours with (left) and without (right) the propeller. $Fr = 0.218$. For the image at the left, $J_S = 0.7$.

4.2 Changes in hull pressure due to the existence of the propeller

Possible pressure changes at the stern of the hull are investigated in this section with the existence of the propeller. It is expected that the propeller changes the pressure distribution of the hull because it changes the flow characteristics, especially at the stern of the ship. The computational work carried out in this section has double body condition. The free surface effects are neglected.

Propeller speeds up the flow at the aft of the ship, creating a negative pressure field at the stern. In figure 10, pressure coefficient along the hull is given. From that figure, it may be observed that the propeller changes the pressure distribution along the hull, especially at the stern.

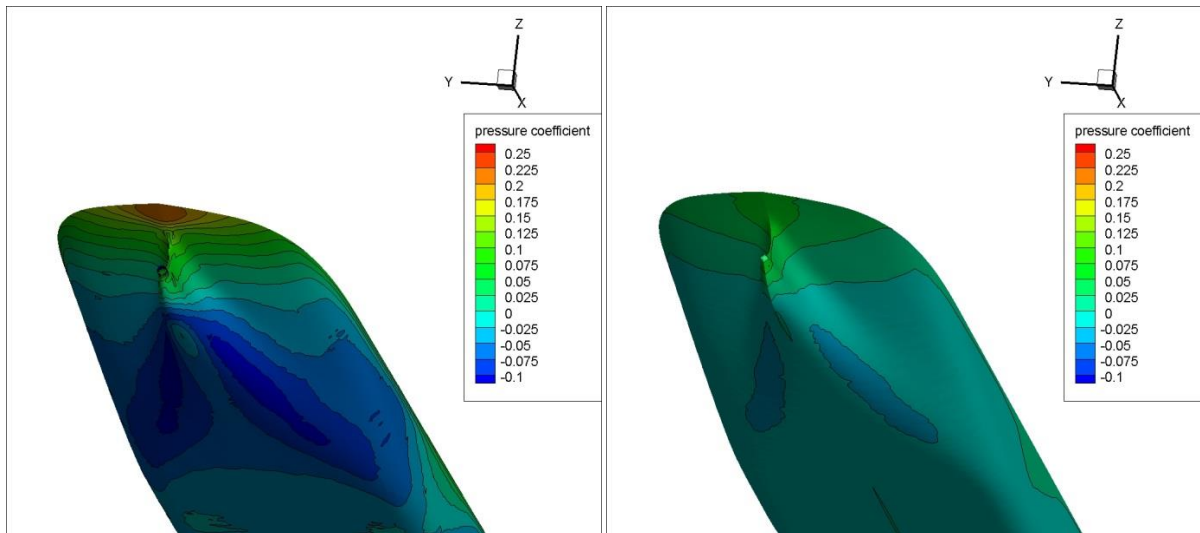


Fig. 10 – Pressure at the aft of the ship at $Fr = 0.218$. With the propeller at $J_S = 0.7$ (left). Without the propeller (right).

The propeller pushes water away by rotating to propel the ship. This rotation speeds up the flow nearby and the stern of the hull is affected by the increased velocity/decreased pressure. The pressure distribution at the left in figure 10 is an end result of the existence of the propeller. This is also in accordance with the decline of wave elevation shown in figure 7. Propeller sucks up the flow to push the vessel. This, in return, reduces the water nearby and air fills in the places evacuated by water, lowering the wave height at the stern of the ship.

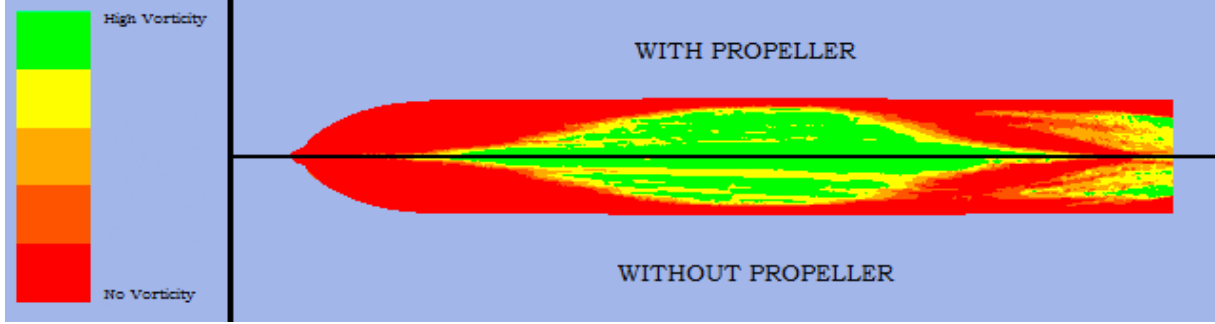


Fig. 11 – Vorticity contours at $Fr = 0.218$ with ($J_S = 0.7$) and without the propeller.

Propeller contributes to the chaotic and turbulent flow at the aft part of the ship. This is due to the fact that while the propeller pushes the water to create thrust, it also rotates to create *swirl* in the flow. Due to this reason, vorticity contours along the hull were investigated. Figure 11 shows the vorticity contours along the hull with and without the propeller. It is found out that although there seems a bit of increase, this is nothing major. The increase in pressure with the existence of the propeller does not seem to contribute much to the vorticity generation at the stern of the ship. The propeller swirl affects the wake of the ship which is downstream but has a smaller effect on the hull which is upstream.

5. Effect of the free surface in ship flow

5.1 Effect of free surface on propeller performance

The free surface effect on the propeller is examined including the hull and therefore its interaction with the propeller. The propeller rotation and therefore the advance coefficient is the same for both cases. The double body flow solutions with the multi-phase results are compared in this section. The effects of cavitation are ignored and the existence of the hull for efficiency compared to open water tests is discussed.

The advance coefficients are calculated for a constant ship velocity and by changing the propeller rotation speed. The Froude number is fixed at $Fr = 0.218$ for the results of the CFD analyses in this section and the ship is not in a self-propulsion state.

Figure 12 reveals the comparison made between the efficiencies calculated for the cases behind the ship hull without the free surface and behind the ship hull with the free surface. It is of direct notice that the efficiency with the ship hull majorly increases and the advance coefficient range widens when figure 12 is compared with the open water propeller test results given in figure 6. To understand why such a difference in results exists, we should write down the equations for the advance coefficient and the efficiency:

$$\text{Advance coefficient: } J_x = \frac{V_x}{n \cdot D} \quad (5)$$

$$\text{Calculated efficiency: } \eta = \frac{J_x K_T}{2\pi K_Q} \quad (6)$$

Here, n is the propeller rotation per second and D is the propeller diameter. K_T is the thrust coefficient while K_Q is the torque coefficient. J_x and V_x refer to advance coefficient and speed of advance respectively. The subscript x may stand for A or S . So V_A in that case, is the flow velocity received by the propeller while V_S is the ship velocity. J_A and J_S take into account velocities V_A and V_S respectively. It should be noted that figure 6 is plotted against J_A which is

calculated by V_A and figure 12 uses J_S to plot the propeller performance with respect to V_S . The relation between V_A and V_S is:

$$V_A = V_S(1 - w) \tag{7}$$

So the relation between J_A and J_S is:

$$J_A = J_S(1 - w) \tag{8}$$

Wake fraction w is always greater than zero. Therefore J_S is greater than J_A which reflects the reason of wider advance coefficient range given in figure 12.

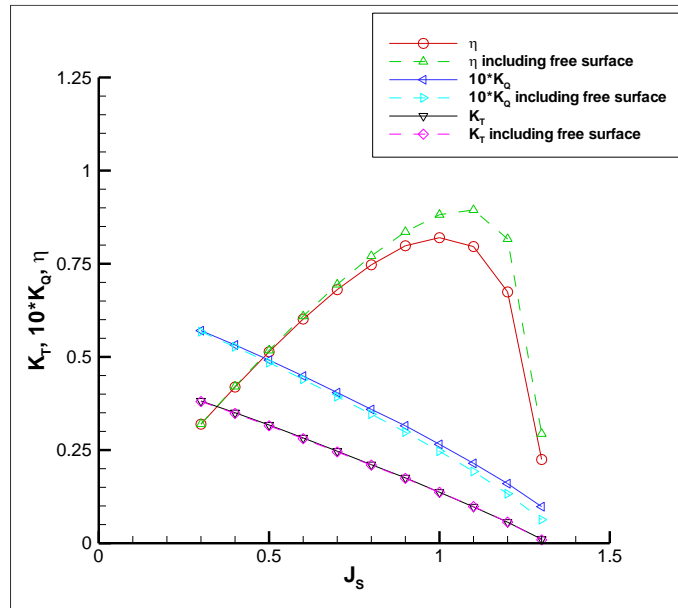


Fig. 12 – Propeller performance with and without the free surface.

The existence of the free surface increases the efficiency of the propeller at higher advance coefficients. This may be examined from figure 12 as there is a clear increasing trend at the efficiency of the propeller after $J = 0.7$. The swirl created by the propeller’s rotation is limited by an upper barrier (which is the free surface in this case) decreasing the torque. The tangential velocities are decreased and the axial velocities are increased. Refer to figure 13 for an effective propeller wake with and without the free surface effect.

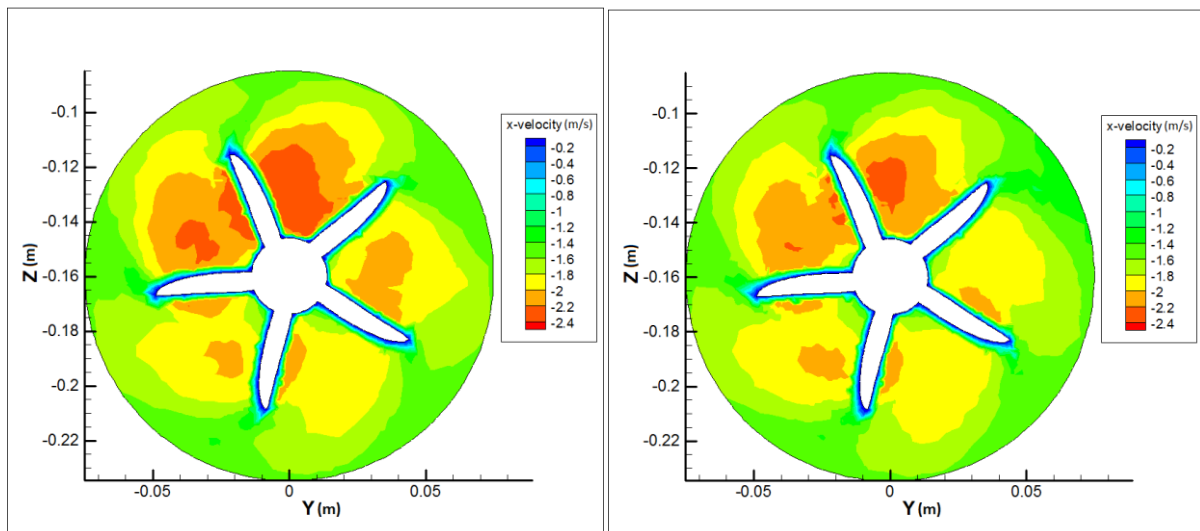


Fig. 13 – Total velocity distribution at the propeller disc with (left) and without (right) the free surface. $J_S = 0.7$, $Fr = 0.218$.

Figure 13 is a proof of the increase in axial velocity when the free surface is present. The free surface behaves like wall in this case and the flow is squeezed between the free surface and the propeller; causing a jet like flow. The increase in thrust and the decrease in torque are very low and hard to perceive from figure 12. The numerical values of K_T , K_Q and η are provided in table 4 so that a greater understanding could be achieved. Here; K_T , K_Q and η are propeller characteristics without the free surface while K_T' , K_Q' and η' are the values obtained with an existing free surface. These small differences reflect on the efficiency of the propeller, especially at higher advance coefficients.

Table 4. Numerical values of K_T , K_Q and η given in figure 12.

J_S	K_T	K_T'	$10*K_Q$	$10*K_Q'$	h	h'
0.3	0.3817	0.3802	0.5706	0.5676	0.3194	0.3198
0.4	0.3503	0.3482	0.5321	0.527	0.4191	0.4207
0.5	0.3172	0.3152	0.4914	0.4847	0.5137	0.5175
0.6	0.2826	0.2805	0.4487	0.4397	0.6016	0.6093
0.7	0.247	0.245	0.4043	0.3931	0.6805	0.6944
0.8	0.2107	0.2096	0.3591	0.3462	0.7471	0.7709
0.9	0.1756	0.1741	0.3152	0.2984	0.7982	0.8356
1	0.1367	0.1367	0.2654	0.2469	0.8199	0.8817
1.1	0.0975	0.0984	0.2144	0.1926	0.7961	0.8944
1.2	0.0564	0.0568	0.1599	0.1328	0.6743	0.8166
1.3	0.0107	0.009	0.0982	0.0632	0.2247	0.2937

The squeeze of the flow between the free surface and the propeller has to be explained further. If this hypothesis is in fact true, then it is expected that the hydrodynamic pressure on the propeller is higher. Figures 14 and 15 show the free surface effect on both sides of the propeller.

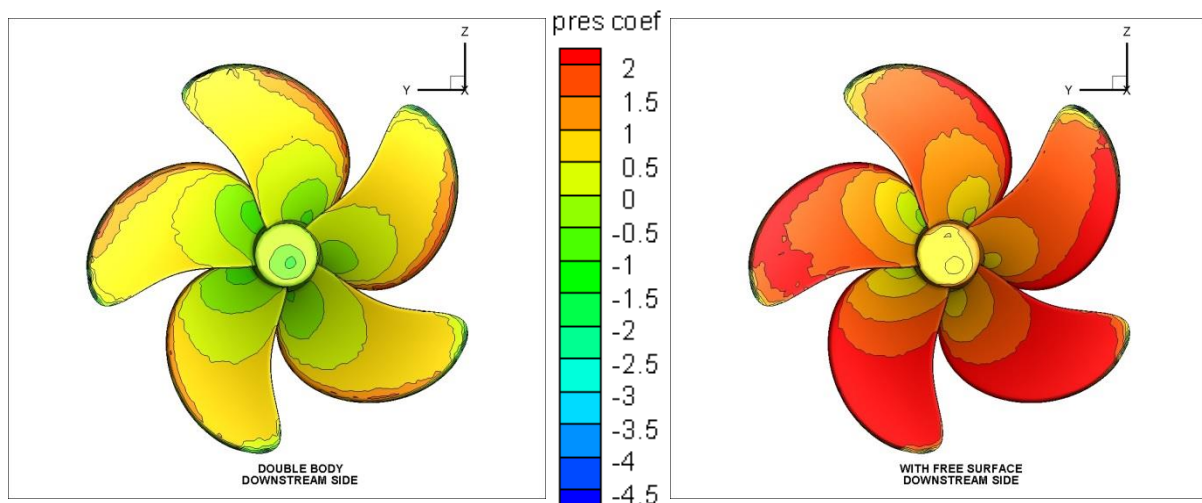


Fig. 14 – Effect of free surface on propeller pressure coefficient distribution at the downstream side. $J_S = 0.7$. Hydrostatic pressure is not included.

The free surface increases the pressure on the propeller as can be seen from figures 14 and 15.

Effects of the hydrostatic pressure are not included when calculating the pressure coefficient to understand how the free surface affects the hydrodynamic pressure. In these graphs pressure is non-dimensionalized by V_S . When the propeller is deeply submerged in water as it is represented by the double body flow solution, it is not affected by the atmospheric pressure. However when there is a free surface nearby, it is oppressed by the atmospheric pressure. It was shown in the previous section that the propeller speeds up the flow to decrease the pressure and the wave height at the stern (please see figures 7 and 10). The decline of the wave height above the propeller will squeeze the flow between the propeller and the free surface to increase the pressure over the propeller. Figures 14 and 15 explain the increase of calculated efficiency given in figure 12.

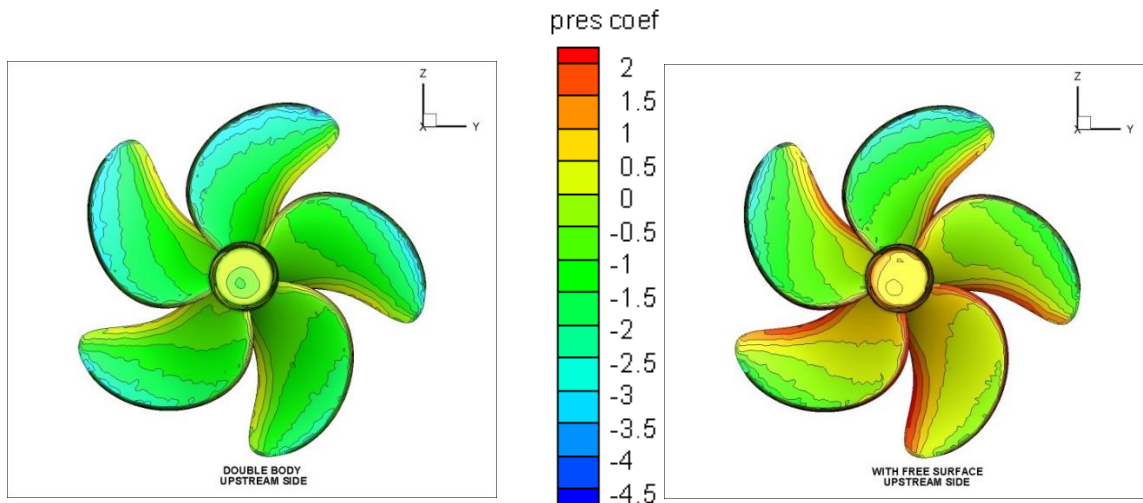


Fig. 15 – Effect of free surface on propeller pressure coefficient distribution at the upstream side. $J_S = 0.7$. Hydrostatic pressure is not included.

Paik et al. [16] experimentally and computationally measured the pressure coefficient distributions of a propeller-ship hull system at ballast and design drafts. They have found out that, when the ship is in ballast draft, the pressure on the propeller is higher. The reason why the pressure on the propeller is lower at design draft is because the propeller is submerged deeper in this case. It is less affected by the free surface than when it is at ballast draft.

5.2 Changes in hull pressure due to the existence of the free surface

The pressure changes in hull with the existence of the free surface are investigated. The propeller is absent in these simulations and has no effect on flow characteristics. The observations are made for the design speed of the vessel.

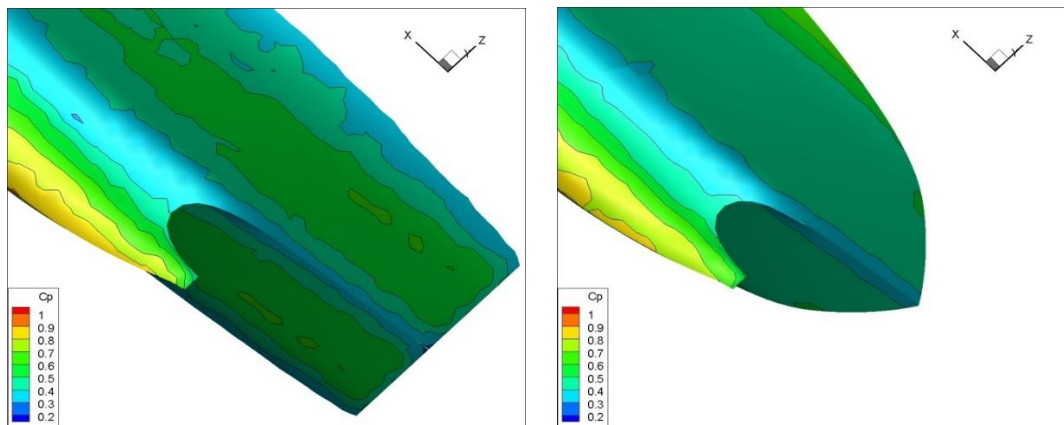


Fig. 16 – Pressure coefficient distribution along the underwater hull with (right) and without (left) the free surface. Hydrostatic pressure is not included. $Fr = 0.218$.

Existence of free surface generally increases the total pressure at the stern of the hull. This may be examined from figure 16 where the effects of the hydrostatic pressure are not included in the total pressure. The reason for this is to accommodate the multiphase solutions with the double body solutions, where the hull is deeply submerged and has no hydrostatic pressure acting upon it. The two ships might seem to have different geometries but this is not the case. For the case without the free surface there is (naturally) no wave elevation while for the case with the free surface, the ship floats between wave crests and troughs. The wave crest at the transom can clearly be seen from the case with the free surface (please see figure 7 for the wave crest at the transom). The effect of the free surface on the hull is compatible with the free surface effect on the propeller. It may be said that the free surface creates an additional pressure over the bodies inside the flow.

6. Conclusion

In this study; hydrodynamics of a benchmark ship, Duisburg Test Case, is computationally investigated. The changes in ship resistance and the propulsion efficiency are observed with the existence of the free surface and the propeller. The computational results are first verified by a widely used methodology within the field and then the generated results are demonstrated. The paper covers the effect of two different changes in the flow. The first one is the existence of the propeller and the second one is the existence of the free surface.

In the first part of the paper it is found out that the existence of the propeller

- lowers the wave elevation at the stern of the hull while increasing it at the bow,
- causes the ship to generate higher waves close to the ship hull and changes the wake field considerably,
- increases the pressure resistance of the ship,
- decreases the pressure at the hull stern and
- does not have a significant effect on vorticity generation along the hull.

The second part covers the effect of the free surface. It is found out that the free surface

- increases the efficiency of the propeller especially at higher advance coefficients,
- increases the pressure on the propeller and
- increases the pressure at hull stern.

Acknowledgments

Authors are grateful to Prof. Fahri Celik from Yildiz Technical University for his valuable recommendations. We also would like to thank the reviewers for their constructive comments and suggestions to improve this paper.

REFERENCES

- [1] Larsson, L., Stern, F., and Bertram, V., 2003, "Benchmark of Computational Fluid Dynamics for Ship Flows: The Gothenburg 2000 Workshop," *Journal of Ship Research*, 47(1), pp. 63-81.
- [2] El Moctar, O., Shigunov, V., and Zorn, T., 2012, "Duisburg Test Case: Post-Panamax Container Ship for Benchmarking," *Ship Technology Research*, 59(3), pp. 50-65.
- [3] Johansson, S. H., Davidson, L., and Olsson, E., 1993, "Numerical simulation of vortex shedding past triangular cylinders at high Reynolds number using a $k-\epsilon$ turbulence model," *International Journal of Numerical Methods in Fluids*, 16(10), pp. 859-878.
- [4] Rhee, S. H., Makarov, B. P., Krishinan, H., and Ivanov, V., 2005, "Assessment of the volume of fluid method for free-surface wave flow," *Journal of Marine Science and Technology*, 10(4), pp. 173-180.
- [5] Hirt, C. W., and Nichols, B., 1981, "Volume of Fluid (VOF) method for the dynamics of free boundaries," *Journal of Computational Physics*, 39(1), pp. 201-225.
- [6] Stern, F., Wilson, R. V., Coleman, H. W., and Paterson, E. G., 2001, "Comprehensive Approach to Verification and Validation of CFD Simulations – Part 1: Methodology and Procedures," *Journal of Fluids Engineering – Transactions of the ASME*, 123(4), pp. 793-802.
- [7] Stern, F., Wilson, R. V., Coleman, H. W., and Paterson, E. G., 2001, "Comprehensive Approach to Verification and Validation of CFD Simulations – Part 2: Application for RANS Simulation of a Cargo/Container ship," *Journal of Fluids Engineering – Transactions of the ASME*, 123(4), pp. 803-810.
- [8] Ogiwara, S., Kajitani, H., 1994, "Pressure Distribution on the Hull Surface of Series 60 (CB=0.60) Model," *Proceedings of CFD Workshop, Tokyo*, 1, pp. 350-358.
- [9] Toda, Y., Stern, F., and Longo, J., 1992, "Mean-Flow Measurements in the Boundary Layer and Wake and Wave Field of a Series 60 CB=.6 Model Ship – Part 1: Froude Numbers .16 and .316," *Journal of Ship Research*, 36(4), pp. 360-377.
- [10] ITTC 7.5-03-02-03, 2011. Recommended Procedures and Guidelines, Practical Guidelines for Ship CFD Applications, Revision 01.
- [11] ITTC 7.5-02-03-01.4, 2011. Recommended Procedures and Guidelines, 1978 ITTC Performance Prediction Method, Revision 02.
- [12] Seo, J. H., Seol, D. M., Lee, J. H., and Rhee, S. H., 2010, "Flexible CFD Meshing Strategy for Prediction of Ship Resistance and Propulsion Performance," *International Journal of Naval Architecture and Ocean Engineering*, 2(3), pp. 139-145.
- [13] Maki, K. J., Broglia, R., Doctors, L. J., and Di Mascio, A., 2012, "Nonlinear wave resistance of a two-dimensional pressure patch moving on a free surface," *Ocean Engineering*, 39, pp. 62-71.
- [14] Kinaci, O. K., Sukas, O. F., and Bal, S., 2015, "Prediction of wave resistance by a Reynolds-averaged Navier-Stokes equation-based computational fluid dynamics approach," *Proceedings of the Institution of Mechanical Engineers; Part M: Journal of Engineering for the Maritime Environment*, published online.
- [15] Kinaci, O. K., Kukner, A., and Bal, S., 2013, "On propeller characteristics of DTC Post-Panamax Container Ship," *International Journal of Ocean System Engineering*, 3(2), pp. 77-89.
- [16] Paik, K. J., Park, H. G., and Seo, J., 2013, "RANS simulation of cavitation and hull pressure fluctuation for marine propeller operating behind-hull condition," *International Journal of Naval Architecture and Ocean Engineering*, 5(4), pp. 502-512.

Submitted: 19.02.2015.

Omer Kemal KINACI, kinaci@yildiz.edu.tr

Accepted: 13.11.2015.

Metin Kemal GOKCE, mkgokce@yildiz.edu.trNaval Architecture and Maritime Faculty, Yildiz Technical University
Istanbul / TURKEY